Supplementary Information for

A Highly Birefringent Metal-Free Crystal Assembled by Cooperative Non-Covalent Interactions

Yanqiang Li,[1] Yang Zhou,[1,2] Belal Ahmed,[1,4] Qianting Xu,[1] Weiqi Huang,[1] Yipeng Song,[1,2] Xianyu Song,[1] Bin Chen,[1] Junhua Luo[1,2,3] Sangen Zhao*[,1,2,3]

[1]State Key Laboratory of Structural Chemistry, Fujian Institute of Research on the Structure of Matter, Chinese Academy of Sciences, Fuzhou, Fujian 350002, China

[2]University of Chinese Academy of Sciences, Beijing 100049, China

[3]Fujian Science & Technology Innovation Laboratory for Optoelectronic Information of China, Fujian 350108, China

*Correspondence to: zhaosangen@fjirsm.ac.cn

CONTENTS

Reagents

Melamine (Adamas, 99%) and KOH (Greagent, ≥90%) were purchased from Tansoole. $NH_3 \cdot H_2O$ (25.0%–28.0%) and HCl (36.0%–38.0%) were purchased from Sinopharm Chemical Reagent Co., Ltd.

Synthesis

Firstly, bulk melon was obtained by the traditional solid-state method. The as-purchased melamine was thoroughly ground, slowly heated to 523 K at a rate of 2 K min^{-1}, and sintered at 523 K for 540 min. The sample was further heated to 658 K at a rate of 1 K min^{-1}, and sintered at 658 K for about 3000 min, resulting in the formation of a light-yellow final product. Secondly, $K_3C_6N_7O_3 \cdot 3H_2O$[1] was synthesized according to the previous report through refluxing melon powder in KOH aqueous solution (2.5 M). After that, $H_3C_6N_7O_3 \cdot 3H_2O$[2] was synthesized by mixing the solution of $K_3C_6N_7O_3 \cdot 3H_2O$ and HCl. Subsequently, $NH_3 \cdot H_2O$ was added drop-wise to the $H_3C_6N_7O_3 \cdot 3H_2O$ solution, and the resulting solution was evaporated at room temperature. Colorless $NH_4(H_2C_6N_7O_3) \cdot 2H_2O$ crystals were successfully grown after several weeks.

Single-Crystal Structure Determination

A colorless slice-shaped $NH_4(H_2C_6N_7O_3) \cdot 2H_2O$ crystal with dimensions 0.12 × 0.09 × 0.02 mm^3 was selected for the single-crystal X-ray diffraction (XRD) analysis using an optical microscope. The diffraction data was collected using graphite-monochromatized Cu Kα radiation (λ = 1.54184 Å) at 200(2) K with a SuperNova, Dual, Cu at home/near, Atlas diffractometer. The intensity data collection, cell refinement, and data reduction were performed using the CrysAlisPro software (Rigaku, V1.171.41.116a, 2021). Using Olex2,[3,4] the crystal structure was solved with the SHELXS[5] structure solution program using Direct Methods and refined with the Olex2.refine package using NoSpherA2,[6] an implementation of non-spherical atomic form factors in Olex2. All non-hydrogen atoms were refined anisotropically. Most hydrogen atom positions were calculated geometrically and refined using the riding model, but some hydrogen atoms were refined freely. Final refinements include anisotropic displacement parameters. The final crystal structure was verified by the ADDSYM algorithm from the PLATON program,[7] and no

higher symmetry was found. Detailed crystal parameters, data collection, and structure refinement were summarized in Table S1. The atomic coordinates and equivalent isotropic displacement parameters were listed in Table S2. The anisotropic displacement parameters were listed in Table S3. Selected bond lengths and bond angles were presented in Table S4 and S5.

Powder XRD Analysis

Powder XRD measurements of the $NH_4(H_2C_6N_7O_3)\cdot 2H_2O$ sample were carried out on a Rigaku SmartLab high-resolution XRD with the SmartLab Studio II software. The 2θ range was 7°–70° with a scan step width of 0.01° and a scanning rate of 3° min^{-1}.

Thermal Stability

The thermal stability of $NH_4(H_2C_6N_7O_3)\cdot 2H_2O$ was investigated by the thermogravimetric (TG) and differential thermal analysis (DTA) on a NETZSCH STA 449F5 simultaneous thermal analyzer instrument. The powder samples of $NH_4(H_2C_6N_7O_3)\cdot 2H_2O$ were placed in the Al_2O_3 crucible, heated at a rate of 15 K min^{-1} from room temperature to 1173 K. The measurement was carried out in an atmosphere of N_2 flowing.

Semiquantitative microprobe analysis

Semiquantitative microprobe analysis on the $NH_4(H_2C_6N_7O_3)\cdot 2H_2O$ crystal was conducted using a field emission scanning electron microscope (SEM) (Hitachi SU8010) equipped with energy dispersive X-ray spectroscopy (EDS). The EDS data was collected on clean surfaces of the samples, confirming the presence of C, N, and O elements. In addition, the SEM elemental mapping of the $NH_4(H_2C_6N_7O_3)\cdot 2H_2O$ single crystal was also collected on the field emission SEM.

XPS Analysis

The X-ray photoelectron spectroscopy (XPS) was operated on the ESCALAB 250Xi XPS instrument by using Al Kα radiation as the source.

FTIR Analysis

Fourier transform infrared spectroscopy (FTIR) in the wavenumber range of 4000–400 cm^{-1} was recorded on the Bruker Vertex 70 infrared spectrometer.

Raman Analysis

Raman spectroscopy between 3500 and 50 cm^{-1} range was collected on a LabRAM HR Evolution Raman microscope (HORIBA Scientific) with a solid-state laser corresponding to the green light (λ = 532 nm).

UV–Vis–NIR Diffuse Reflectance Spectroscopy

The UV–Vis–NIR diffuse reflection data was recorded at room temperature using a powdered $BaSO_4$ sample as a standard (100% reflectance) on a PerkinElmer Lamda-950 UV–Vis–NIR spectrophotometer. The scanning wavelength range is from 200 nm to 1000 nm. Absorption (*K*/*S*) data was calculated from the following Kubelka–Munk function[8]:

$$F(R) = (1 - R)^2/(2R) = K/S \quad \text{Eq(1)}$$

R is the reflectance, *K* is the absorption, and *S* is the scattering.

Birefringence Tests

The birefringence of $NH_4(H_2C_6N_7O_3)\cdot 2H_2O$ was characterized by the polarized method under the polarized microscope (Nikon ECLIPSE LV100N POL) equipped with a Berek compensator at λ = 550 nm. The relative error is small enough because of the clear boundary lines of the first-, second-, and third-order interference color. In order to improve the accuracy of the birefringence, the small and transparent $NH_4(H_2C_6N_7O_3)\cdot 2H_2O$ crystals were chosen. The formula for calculating the birefringence is listed below:[9,10]

$$R = |n_e - n_o| \times T = \Delta n \times T \quad \text{Eq(2)}$$

Here, *R* represents the optical path difference, Δn is the birefringence, and *T* denotes the thickness of the tested crystal.

Theoretical Calculations

First-principles calculations were conducted using the CASTEP software,[11] a plane-wave pseudopotential package[12] on the basis of the density functional theory (DFT).[13] The exchange-correlation energy was described by the generalized gradient approximation (GGA) scheme of Perdew–Burke–Ernzerhof (PBE) functional, as implemented in the CASTEP code.[14] Before the calculation, atomic positions in the unit cell have been fully geometrically optimized with the aid of the Broyden-Fletcher-Goldfarb-Shannon (BFGS) algorithm.[15] Norm-conserving pseudopotentials were employed to simulate the ion-electron interactions for each atomic specie with following valence configurations: H $1s^1$; C $2s^2 2p^2$; N $2s^2 2p^3$; O $2s^2 2p^4$.[16] A cutoff energy of 1200 eV and the Monkhorst–Pack[17] *k*-point meshes (4 × 1 × 6) spacing less than 0.03 $Å^{-1}$ in the Brillouin zone were chosen for the calculation. Herein, all calculations were performed without the scissors operator. The linear optical properties were examined based on the dielectric function ε, defined by $\varepsilon = N^2$, where $N = n - ik$. Herein, N represents the complex refractive index, n represents the refractive index, and k represents the extinction coefficient.

To explore the polarizability anisotropy of $(H_2C_6N_7O_3)^-$ and other similar π-conjugated birefringent functional units, systematic calculations were implemented via the Gaussian 09 package[18] with the hybrid B3LYP functional at 6-31G(d,p) level. After that, the calculation results were analyzed by the Multiwfn 3.8 code.[19]

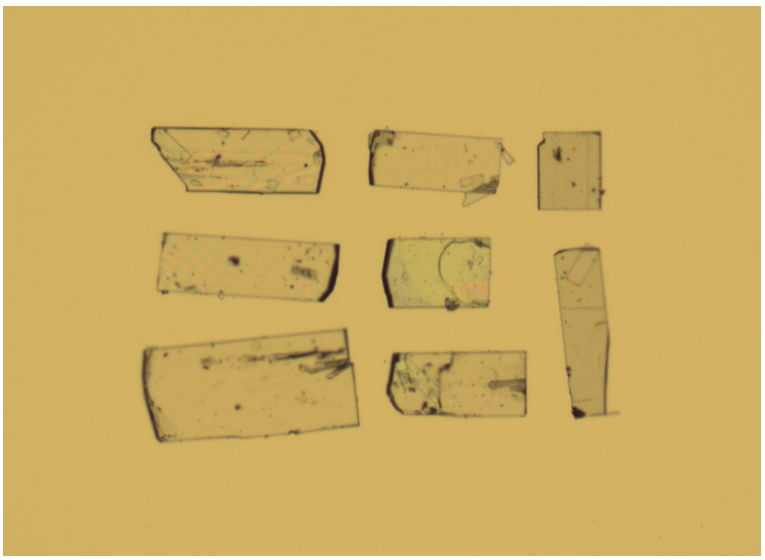

Figure S1. The photograph of as-synthesized $NH_4(H_2C_6N_7O_3)\cdot 2H_2O$ crystals.

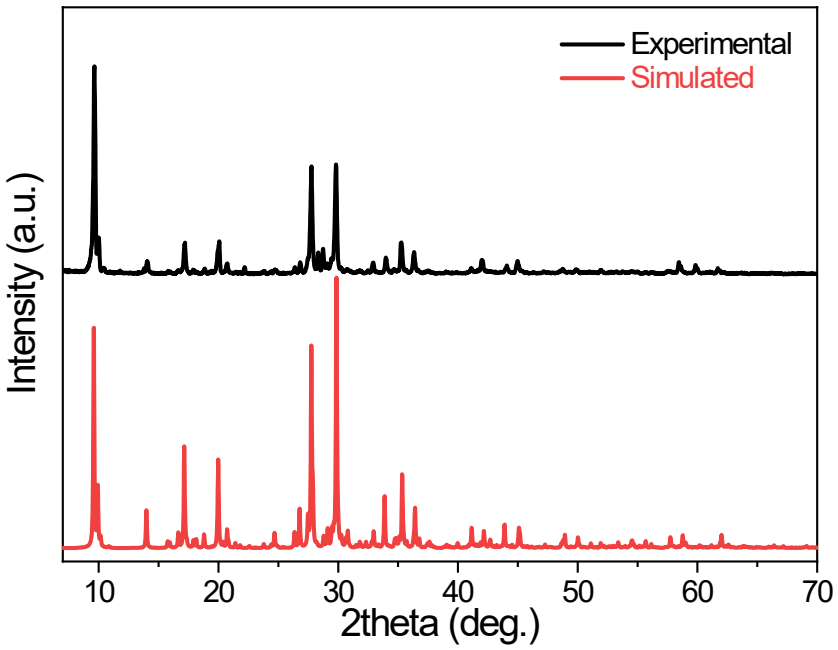

Figure S2. Experimental and simulated powder XRD patterns of $NH_4(H_2C_6N_7O_3)\cdot 2H_2O$.

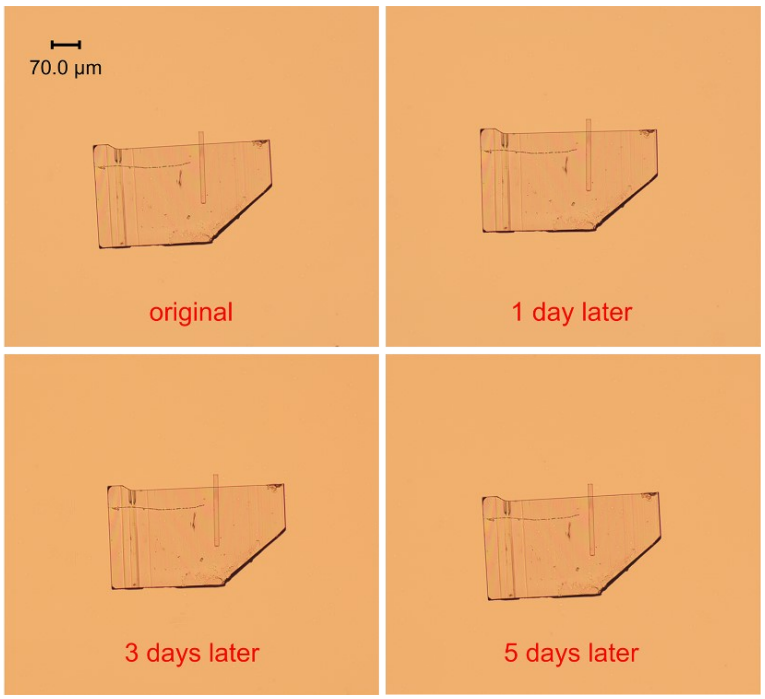

Figure S3. The original single crystal of $NH_4(H_2C_6N_7O_3)\cdot 2H_2O$ and the corresponding single crystal exposed to the air at room temperature for one day, three days, and five days observed under the optical microscope.

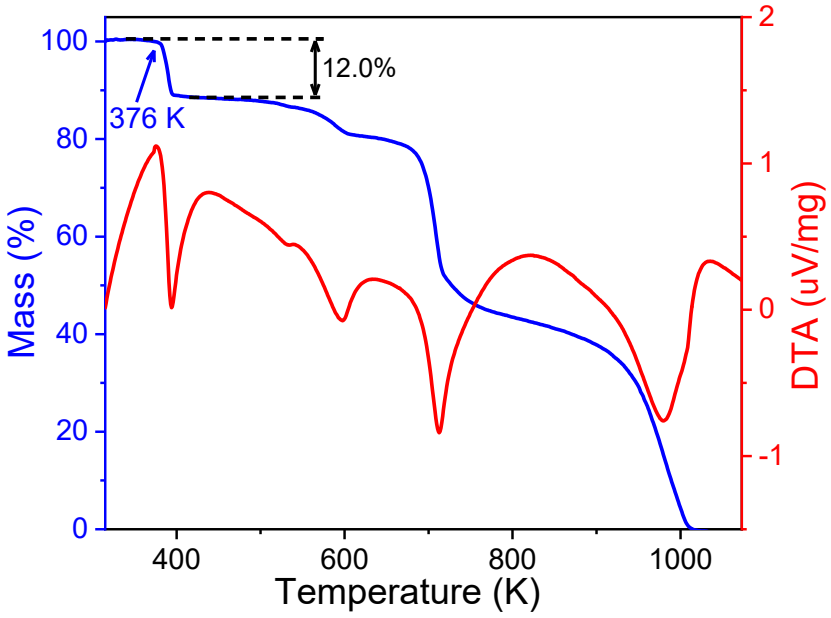

Figure S4. TG and DTA curves of $NH_4(H_2C_6N_7O_3)\cdot 2H_2O$.

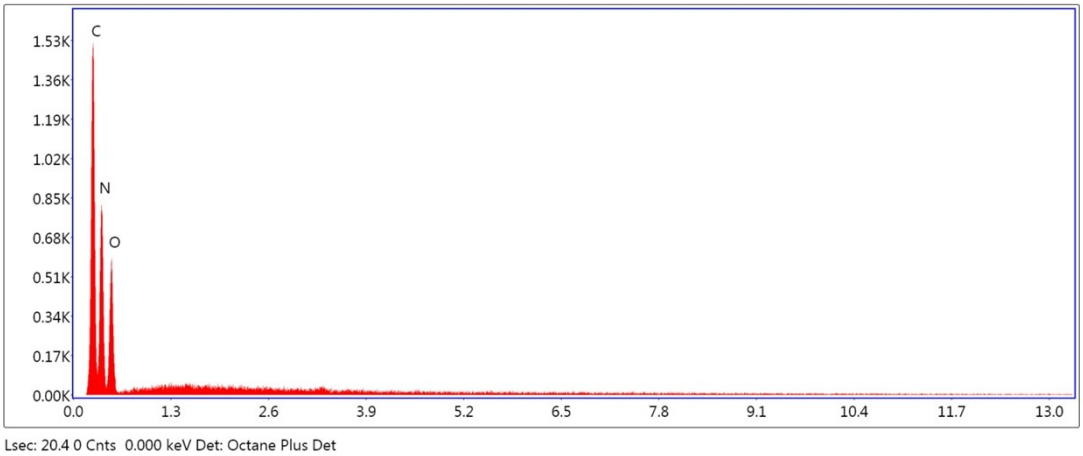

Figure S5. EDS result of $NH_4(H_2C_6N_7O_3)\cdot 2H_2O$.

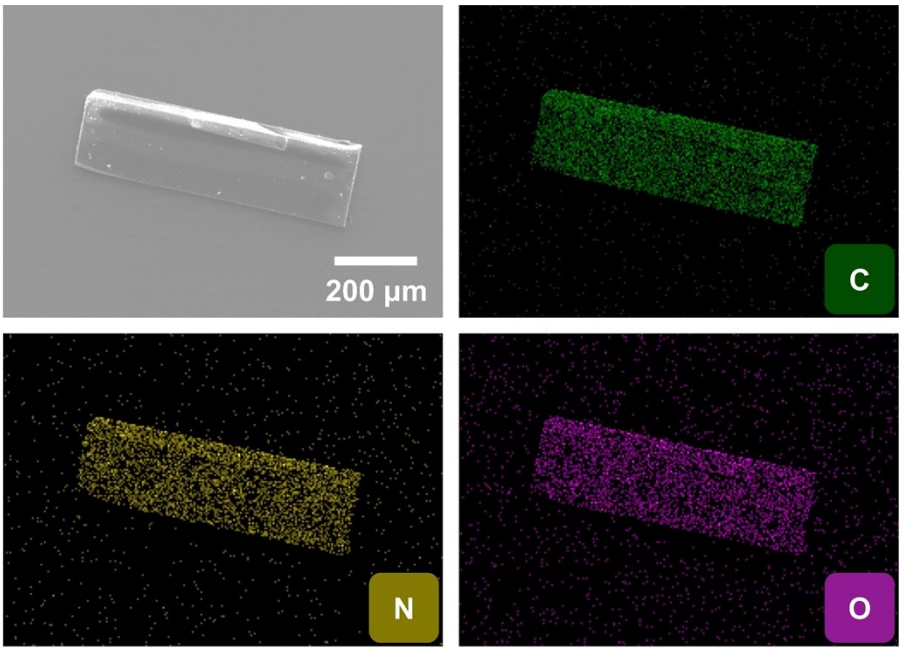

Figure S6. The elemental mapping. Scale bar, 200 μm.

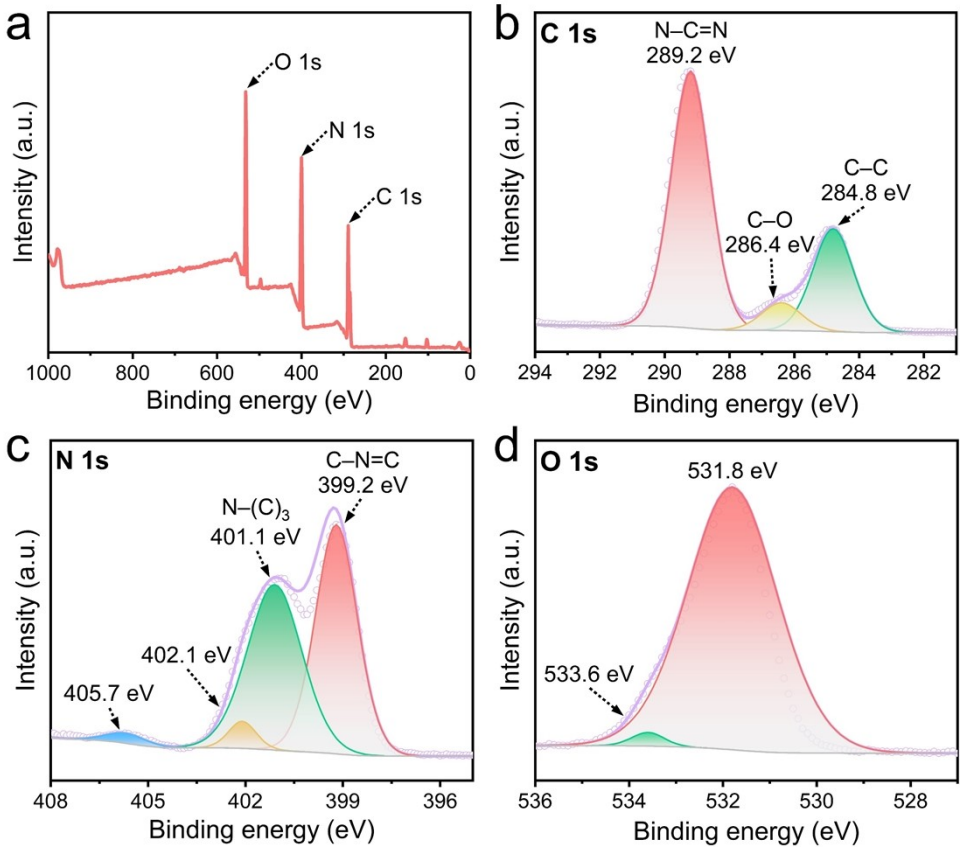

Figure S7. (a) The XPS survey scan for $NH_4(H_2C_6N_7O_3)\cdot 2H_2O$. (b), (c), and (d) High-resolution XPS spectra of C 1s, N 1s, and O 1s.

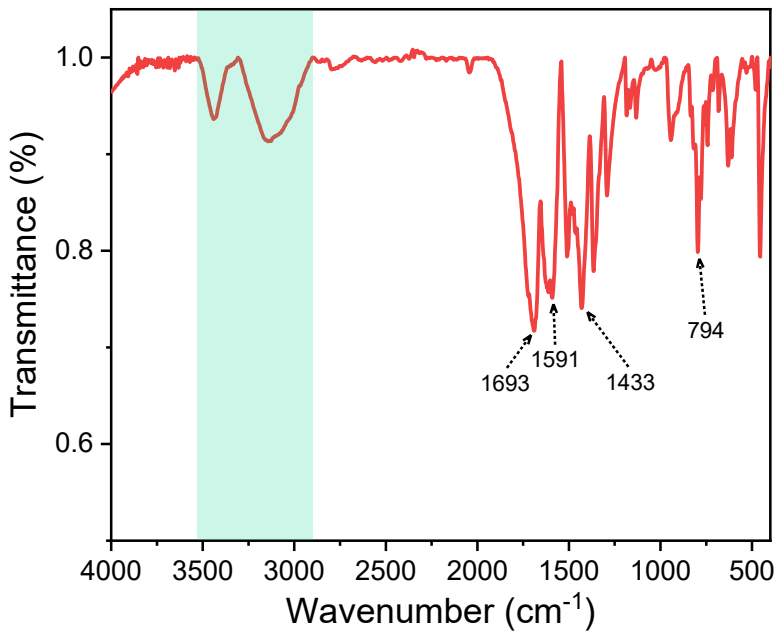

Figure S8. FTIR of $NH_4(H_2C_6N_7O_3)\cdot 2H_2O$.

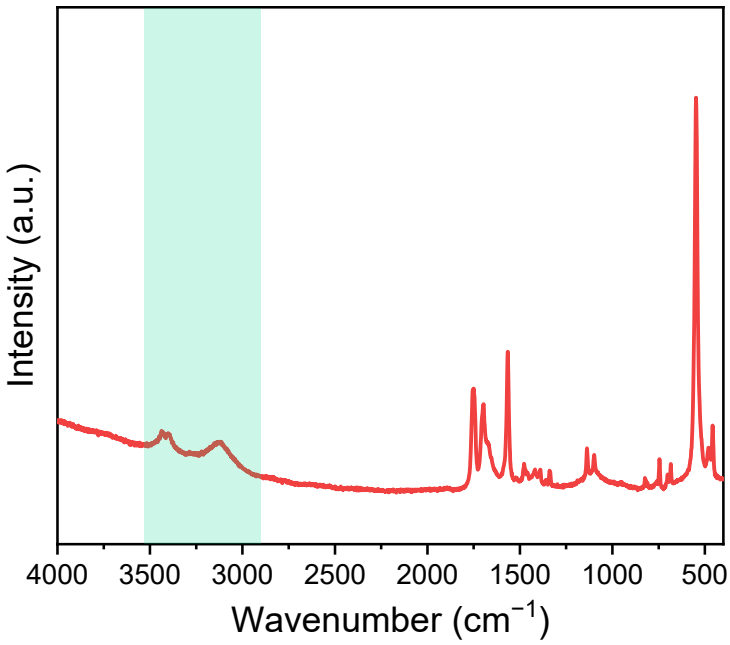

Figure S9. Raman spectrum of $NH_4(H_2C_6N_7O_3)\cdot 2H_2O$.

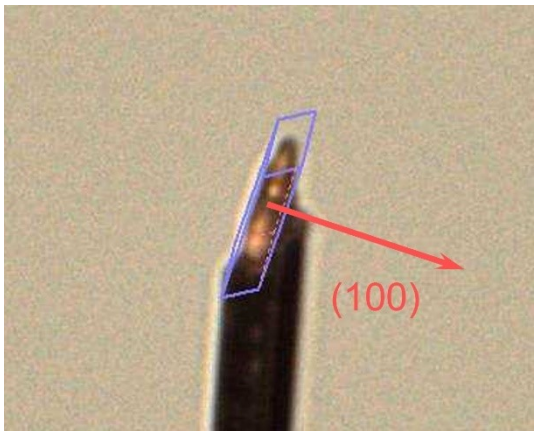

Figure S10. The crystal orientation of the selected $NH_4(H_2C_6N_7O_3)\cdot 2H_2O$ plate determined by single-crystal XRD.

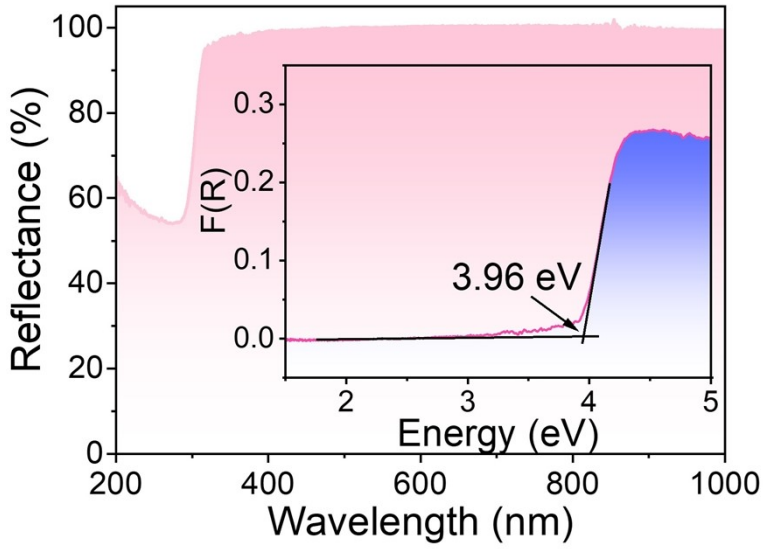

Figure S11. The UV–Vis–NIR diffuse reflectance spectrum of $NH_4(H_2C_6N_7O_3)\cdot 2H_2O$. The inset represents the experiment bandgap.

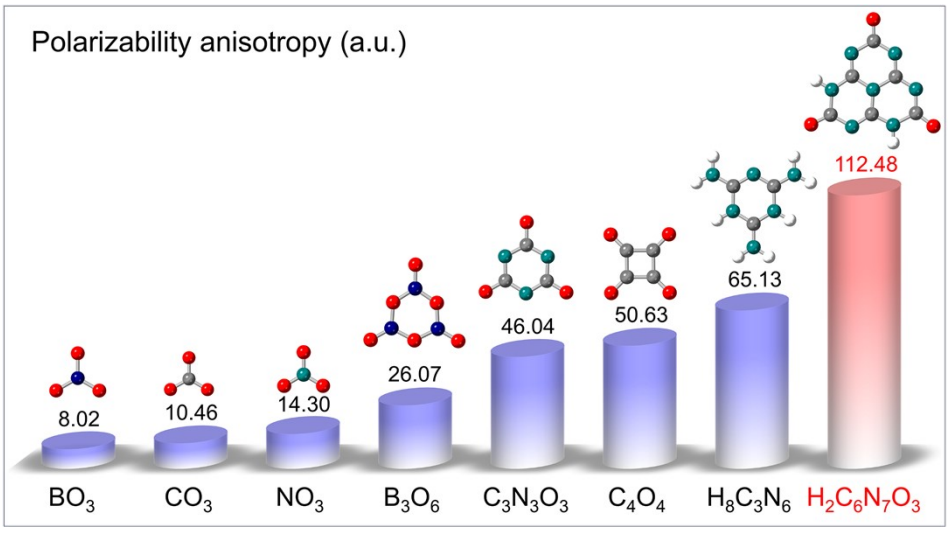

Figure S12. Polarizability anisotropy of π-conjugated birefringent functional units $(BO_3)^{3-}$, $(CO_3)^{2-}$, $(NO_3)^{-}$, $(B_3O_6)^{3-}$, $(C_3N_3O_3)^{3-}$, $(C_3H_8N_6)^{2+}$, $(C_4O_4)^{2-}$, and $(H_2C_6N_7O_3)^{-}$.

Table S1. Crystal data and structure refinement for $NH_4(H_2C_6N_7O_3)\cdot 2H_2O$.

Empirical formula	$NH_4(H_2C_6N_7O_3)\cdot 2H_2O$
Formula weight	274.22
Shape	slice-shaped
Size/mm^3	0.12 × 0.09 × 0.02
Temperature/K	200(2)
Crystal system	monoclinic
Space group	$P2_1/c$
a/Å	9.2242(2)
b/Å	34.8178(7)
c/Å	6.42910(1)
α/°	90
β/°	92.597(2)
γ/°	90
Volume/Å^3	2062.69(7)
Z	4
Z'	1
ρ(g cm^{-3})	1.766
μ/mm^{-1}	1.338
F(000)	1136.0
Radiation	Cu Kα (λ = 1.54184 Å)
2θ range for data collection/°	9.598 to 144.83
Index ranges	$-11 \le h \le 11$, $-42 \le k \le 40$, $-7 \le l \le 5$
Reflections collected	9189
Independent reflections	3980 (R_{int} = 0.0272, R_{sigma} = 0.0268)
Data/restraints/parameters	3980/3/524
Goodness-of-fit on F^2	1.0939
Final R indexes [I≥2σ(I)][a]	R_1 = 0.0241, wR_2 = 0.0625
Final R indexes [all data][a]	R_1 = 0.0312, wR_2 = 0.0669
Largest diff. peak/hole / e Å^{-3}	0.24/−0.19

[a]$wR_1 = \Sigma||F_o|-|F_c||/\Sigma|F_o|$ and $wR_2 = [\Sigma w(F_o^2-F_c^2)^2/\Sigma wF_o^4]^{1/2}$ for $F_o^2 > 2\sigma(F_o^2)$.

Table S2. Atomic coordinates (× 10^{-4}) and equivalent isotropic displacement parameters (Å^2 × 10^3) for $NH_4(H_2C_6N_7O_3)\cdot 2H_2O$.

Atom	*x*	*y*	*z*	U_{eq}[a]
O1	8634.2(8)	5230.8(2)	1090.4(11)	22.33(17)
O2	1590.4(8)	1590.4(8)	1590.4(8)	1590.4(8)
O3	5075.1(8)	5075.1(8)	5075.1(8)	5075.1(8)
O4	3499.3(8)	5586.1(2)	-1963.4(11)	22.03(17)
O5	50.7(8)	50.7(8)	50.7(8)	50.7(8)
O6	7103.1(8)	7269.6(2)	-3388.4(12)	22.03(16)
O7	8652.6(9)	6311.1(3)	-1820.1(15)	24.02(18)
O8	9993.8(9)	6121.9(3)	3961.7(16)	28.00(19)
O9	6992.4(9)	5593.5(3)	6432.3(12)	21.62(17)
O10	1575.6(9)	6901.0(3)	4030.5(13)	22.65(17)
N1	6292.4(9)	5221.4(3)	1944.6(12)	15.24(17)
N2	7565.5(8)	5809.0(2)	1585.8(12)	14.63(17)
N3	3920.1(9)	5196.9(2)	2894.8(12)	15.62(17)
N4	5094.0(8)	5792.9(2)	2440.7(11)	11.34(17)
N5	6371.7(9)	6374.5(2)	2162.0(12)	14.62(17)
N6	2669.0(9)	5787.6(2)	3225.8(12)	15.02(17)
N7	3815.5(9)	6369.5(2)	2824.8(12)	14.47(17)
N8	4799.1(9)	6127.7(2)	-2383.7(12)	14.56(17)
N9	2235.9(9)	6137.9(2)	-1772.6(12)	14.67(17)
N10	6034.4(9)	6693.4(2)	-2822.7(12)	14.74(17)
N11	3566.2(8)	6712.7(2)	-1988.9(11)	11.48(17)
N12	1139.1(10)	6722.4(2)	-1244.9(13)	15.57(18)
N13	2427.2(9)	7309.9(2)	-1432.0(12)	14.76(17)
N14	4798.7(9)	7282.5(3)	-2375.5(12)	15.05(17)
N15	8563.7(12)	6997.8(3)	3036.1(18)	22.7(2)
N16	10029.2(12)	5476.1(3)	7384.5(19)	20.1(2)
C1	7572.4(10)	5418.3(3)	1516.4(14)	14.41(19)
C2	5060.6(10)	5394.9(3)	2444.5(13)	12.00(19)
C3	6374.2(10)	5997.0(3)	2061.5(13)	11.96(19)

Atom	*x*	*y*	*z*	U_{eq}[a]
C4	2674.9(10)	5388.6(3)	3357.5(14)	15.04(19)
C5	3855.8(10)	5996.8(3)	2835.5(13)	12.10(19)
C6	5102.4(10)	6565.0(3)	2485.8(13)	14.0(2)
C7	1144.9(10)	7120.8(3)	-1082.0(14)	14.66(19)
C8	2302.1(10)	6510.7(3)	-1679.9(13)	12.25(18)
C9	3552.2(10)	7110.5(3)	-1905.8(13)	11.86(19)
C10	3519.3(10)	5941.2(3)	-2045.5(13)	14.0(2)
C11	4831.4(10)	6507.4(3)	-2415.0(12)	11.69(19)
C12	6048.1(10)	7083.6(3)	-2892.9(14)	14.59(19)
H1	6338(17)	4928(5)	1930(20)	30(4)
H6	1712(16)	5924(5)	3500(20)	30(4)
H7a	7770(20)	6442(5)	-2280(30)	38(4)
H7b	8350(20)	6142(6)	-670(30)	50(5)
H8a	9190(20)	6012(6)	3090(30)	39(5)
H8b	9630(30)	6217(6)	5210(30)	69(7)
H9a	6320(20)	5781(5)	6910(30)	39(4)
H9b	6560(20)	5337(6)	6730(30)	44(5)
H10a	1985(19)	7150(5)	3820(20)	34(4)
H10b	2240(20)	6714(5)	3510(30)	34(4)
H12	190(20)	6587(5)	-1200(20)	42(4)
H14	4835(18)	7577(5)	-2410(30)	38(4)
H15a	7921(18)	6757(5)	2570(20)	26(4)
H15b	9620(20)	6923(5)	3360(30)	43(4)
H15c	8150(20)	7088(6)	4310(40)	77(7)
H15d	8490(30)	7193(7)	1970(30)	75(7)
H16a	8930(20)	5540(5)	7090(20)	32(4)
H16b	10600(20)	5703(6)	7810(30)	43(4)
H16c	10420(30)	5398(6)	6110(40)	70(6)
H16d	10130(30)	5304(9)	8360(40)	104(10)

[a]U_{eq} is defined as one-third of the trace of the orthogonalized U_{ij} tensor.

Table S3. Anisotropic displacement parameters ($Å^2 \times 10^{-3}$) for $NH_4(H_2C_6N_7O_3)\cdot 2H_2O$.

Atom	*U*11	*U*22	*U*33	*U*23	*U*13	*U*12
O1	17.2(4)	16.3(4)	34.1(4)	5.5(3)	7.9(3)	3.2(3)
O2	16.0(3)	14.9(3)	37.9(4)	-4.0(3)	8.4(3)	-3.3(3)
O3	25.1(4)	7.1(3)	33.0(4)	0.7(3)	-1.0(3)	0.2(3)
O4	25.1(4)	7.3(3)	33.5(4)	0.5(3)	-0.7(3)	0.6(3)
O5	16.0(3)	15.8(3)	35.2(4)	4.1(3)	8.3(3)	1.7(3)
O6	16.1(3)	16.2(4)	34.4(4)	-4.6(3)	8.2(3)	-2.8(3)
O7	13.1(4)	19.1(4)	40.0(5)	-1.3(3)	3.0(3)	2.0(4)
O8	17.3(4)	24.8(4)	41.4(5)	0.5(3)	-3.7(4)	-5.9(4)
O9	18.7(4)	16.6(4)	29.6(4)	1.2(3)	1.7(3)	-1.3(3)
O10	19.4(4)	15.6(4)	33.1(4)	0.8(4)	2.9(3)	0.2(4)
N1	14.5(4)	8.9(4)	22.5(4)	1.3(3)	3.0(3)	-1.0(3)
N2	12.3(4)	10.9(4)	20.7(4)	0.4(3)	2.0(3)	0.5(3)
N3	14.6(4)	8.6(4)	24.0(4)	-0.6(3)	3.7(3)	-0.4(3)
N4	12.1(4)	7.2(4)	14.7(4)	0.2(3)	0.2(3)	-0.4(3)
N5	15.5(4)	8.7(4)	19.7(4)	-0.9(3)	0.7(3)	-0.6(3)
N6	12.8(4)	10.9(4)	21.5(4)	0.7(3)	1.5(3)	0.5(3)
N7	15.1(4)	8.3(4)	19.9(4)	2.6(3)	0.2(3)	-0.8(3)
N8	15.0(4)	7.8(4)	20.7(4)	2.0(3)	0.0(3)	-0.4(3)
N9	14.6(4)	8.6(4)	20.8(4)	-1.7(3)	0.3(3)	-0.1(3)
N10	11.8(4)	11.1(4)	21.3(4)	0.8(3)	1.9(3)	-0.3(3)
N11	11.2(4)	7.1(4)	16.1(4)	-0.0(3)	0.7(3)	-0.2(3)
N12	12.2(4)	12.0(4)	22.7(4)	-0.3(3)	2.7(3)	-0.3(3)
N13	14.1(4)	8.1(4)	22.3(4)	1.2(3)	3.9(3)	-0.8(3)
N14	13.5(4)	9.5(4)	22.4(4)	-1.1(3)	3.3(3)	-0.3(3)
N15	17.6(5)	18.2(5)	32.5(6)	-2.8(4)	3.9(4)	0.1(4)
N16	16.6(5)	16.9(5)	27.0(6)	-1.0(4)	4.6(4)	3.1(4)
C1	13.9(4)	11.5(4)	18.1(4)	2.2(4)	2.4(3)	1.3(3)
C2	13.0(4)	8.0(4)	15.0(4)	0.0(3)	0.7(3)	-0.2(3)
C3	12.2(4)	9.0(4)	14.7(4)	-0.5(3)	-0.1(3)	0.0(3)
C4	14.1(4)	11.1(4)	20.0(4)	-1.6(4)	1.8(3)	-1.0(4)

Atom	*U*11	*U*22	*U*33	*U*23	*U*13	*U*12
C5	12.5(4)	9.7(4)	13.9(4)	1.3(3)	-0.7(3)	-0.6(3)
C6	17.5(5)	8.2(5)	16.2(4)	0.0(4)	-2.1(3)	-0.2(3)
C7	13.2(4)	11.8(4)	19.1(4)	1.9(4)	1.7(3)	0.5(3)
C8	13.2(4)	8.4(4)	15.0(4)	-0.4(3)	-0.4(3)	0.0(3)
C9	12.2(4)	8.2(4)	15.2(4)	0.1(3)	0.8(3)	-0.9(3)
C10	17.3(5)	8.5(4)	16.1(4)	0.0(3)	-1.8(3)	-0.5(3)
C11	12.3(4)	8.5(4)	14.2(4)	1.0(3)	-0.7(3)	-0.4(3)
C12	13.2(4)	11.6(4)	19.0(4)	-1.3(4)	1.4(3)	-0.5(4)
H1	36(10)	24(10)	30(8)	5(7)	10(7)	0(7)
H6	15(8)	39(10)	36(9)	1(8)	4(7)	5(8)
H7a	32(11)	38(12)	43(10)	5(9)	4(8)	16(9)
H7b	33(11)	59(14)	58(12)	3(10)	18(9)	19(11)
H8a	20(10)	60(14)	35(10)	-3(10)	-17(8)	-19(9)
H8b	92(19)	38(13)	77(15)	25(12)	9(13)	-13(12)
H9a	39(11)	31(10)	48(11)	3(10)	3(9)	-2(9)
H9b	27(11)	55(14)	49(12)	-8(10)	-9(9)	0(11)
H10a	39(11)	33(10)	30(9)	8(9)	9(7)	1(8)
H10b	37(10)	19(9)	46(11)	13(9)	10(8)	-3(8)
H12	52(12)	48(11)	27(8)	16(10)	14(8)	5(8)
H14	37(10)	23(10)	54(11)	-10(8)	6(8)	-6(8)
H15a	27(8)	15(6)	36(9)	-6(3)	-6(6)	3(4)
H15b	38(11)	40(11)	52(11)	0(9)	5(8)	-10(9)
H15c	62(15)	40(13)	130(20)	6(11)	5(15)	-31(14)
H15d	88(18)	63(15)	71(14)	3(13)	-24(12)	33(13)
H16a	30(11)	40(11)	25(9)	1(9)	-3(7)	-4(8)
H16b	50(12)	36(10)	43(10)	0(10)	9(8)	0(9)
H16c	75(16)	62(15)	73(14)	-15(13)	6(12)	-12(12)
H16d	73(17)	150(30)	90(18)	-26(18)	-17(14)	36(18)

Table S4. Selected bond lengths (Å) for $NH_4(H_2C_6N_7O_3)\cdot 2H_2O$.

Selected bonds	Length (Å)	Selected bonds	Length (Å)
O1−C1	1.2186(12)	N10−C11	1.3214(12)
O3−C6	1.2337(13)	N10−C12	1.3595(13)
O2−C4	1.2183(12)	N9−C8	1.3008(12)
O5−C7	1.2124(12)	N9−C10	1.3857(12)
O6−C12	1.2229(12)	N7−C5	1.2980(13)
O4−C10	1.2375(12)	N7−C6	1.3942(12)
N11−C8	1.3837(12)	N6−C5	1.3480(13)
N11−C9	1.3861(12)	N6−C4	1.3918(12)
N11−C11	1.4062(12)	N14−C9	1.3429(12)
N4−C3	1.4089(12)	N14−C12	1.3976(12)
N4−C2	1.3859(12)	N3−C2	1.3013(13)
N4−C5	1.3782(12)	N3−C4	1.3726(12)
N12−C8	1.3415(12)	N8−C11	1.3224(13)
N12−C7	1.3910(13)	N8−C10	1.3732(13)
N2−C3	1.3266(12)	N13−C9	1.2962(12)
N2−C1	1.3611(13)	N13−C7	1.3811(12)
N5−C3	1.3160(13)	N1−C2	1.3389(12)
N5−C6	1.3698(12)	N1−C1	1.4034(12)

Table S5. Selected bond angles (°) for $NH_4(H_2C_6N_7O_3)\cdot 2H_2O$.

Selected bond angles	Angle (˚)	Selected bond angles	Angle (˚)
C8−N11−C9	119.54(8)	N7−C5−N4	122.54(9)
C8−N11−C11	118.80(8)	N7−C5−N6	121.19(9)
C9−N11−C11	121.66(8)	N6−C5−N4	116.27(8)
C2−N4−C3	121.57(8)	N14−C9−N11	115.30(8)
C5−N4−C3	118.69(8)	N13−C9−N11	123.58(8)
C5−N4−C2	119.74(8)	N13−C9−N14	121.11(9)
C8−N12−C7	124.27(9)	N10−C11−N11	120.08(9)
C3−N2−C1	120.38(8)	N8−C11−N11	119.07(8)
C3−N5−C6	119.64(8)	N8−C11−N10	120.85(9)
C11−N10−C12	120.38(8)	O3−C6−N5	119.86(9)
C8−N9−C10	117.42(8)	O3−C6−N7	118.33(9)
C5−N7−C6	117.68(8)	N5−C6−N7	121.80(9)
C5−N6−C4	123.35(9)	O6−C12−N10	123.12(9)
C9−N14−C12	123.80(9)	O6−C12−N14	118.31(9)
C2−N3−C4	118.91(8)	N10−C12−N14	118.57(9)
C11−N8−C10	119.68(8)	O5−C7−N12	119.98(9)
C9−N13−C7	118.92(8)	O5−C7−N13	122.40(9)
C2−N1−C1	123.87(9)	N13−C7−N12	117.62(8)
N12−C8−N11	115.96(8)	O4−C10−N9	118.29(9)
N9−C8−N11	122.60(9)	O4−C10−N8	119.58(9)
N9−C8−N12	121.43(9)	N8−C10−N9	122.13(9)
N2−C3−N4	120.04(9)	O1−C1−N2	123.22(9)
N5−C3−N4	119.47(8)	O1−C1−N1	118.31(9)
N5−C3−N2	120.49(9)	N2−C1−N1	118.47(8)
N3−C2−N4	123.26(9)	O2−C4−N6	119.75(9)
N3−C2−N1	121.17(9)	O2−C4−N3	122.02(9)
N1−C2−N4	115.57(8)	N3−C4−N6	118.24(9)

References

1 Horvath-Bordon, E. *et al.* Alkalicyamelurates, $M_3C_6N_7O_3 \cdot xH_2O$, M = Li, Na, K, Rb, Cs: UV-luminescent and thermally very stable ionic tri-*s*-triazine derivatives. *Dalton Trans.* 3900-3908 (2004).

2 Sattler, A. & Schnick, W. Zur Frage der Tautomerie von Cyamelursäure im Kristall. *Z. Anorg. Allg. Chem.* **632**, 1518-1523 (2006).

3 Dolomanov, O. V., Bourhis, L. J., Gildea, R. J., Howard, J. A. K. & Puschmann, H. OLEX2: a complete structure solution, refinement and analysis program. *J. Appl. Crystallogr.* **42**, 339-341 (2009).

4 Bourhis, L. J., Dolomanov, O. V., Gildea, R. J., Howard, J. A. K. & Puschmann, H. The anatomy of a comprehensive constrained, restrained refinement program for the modern computing environment-Olex2 dissected. *Acta Crystallogr., Sect. A: Found. Adv.* **71**, 59-75 (2015).

5 Sheldrick, G. M. A short history of SHELX. *Acta Crystallogr., Sect. A: Found. Adv.* **64**, 112-122 (2008).

6 Kleemiss, F. *et al.* Accurate crystal structures and chemical properties from NoSpherA2. *Chem. Sci.* **12**, 1675-1692 (2021).

7 Spek, A. L. Single-crystal structure validation with the program PLATON. *J. Appl. Crystallogr.* **36**, 7-13 (2003).

8 Tauc, J. Absorption edge and internal electric fields in amorphous semiconductors. *Mater. Res. Bull.* **5**, 721-729 (1970).

9 Cao, L. *et al.* A microcrystal method for the measurement of birefringence. *Crystengcomm* **22**, 1956-1961 (2020).

10 Sorensen, B. E. A revised Michel-Levy interference colour chart based on first-principles calculations. *Eur. J. Mineral.* **25**, 5-10 (2013).

11 Clark, S. J. *et al.* First principles methods using CASTEP. *Z. Kristallogr.* **220**, 567-570 (2005).

12 Payne, M. C., Teter, M. P., Allan, D. C., Arias, T. A. & Joannopoulos, J. D. Iterative minimization techniques for ab initio total-energy calculations: molecular dynamics and conjugate gradients. *Rev. Mod. Phys.* **64**, 1045-1097 (1992).

13 Kohn, W. & Sham, L. J. Self-Consistent Equations Including Exchange and Correlation Effects. *Phys. Rev.* **140**, 1133-& (1965).

14 Perdew, J. P., Burke, K. & Ernzerhof, M. Generalized Gradient Approximation Made Simple. *Phys. Rev. Lett.* **77**, 3865-3868 (1996).

15 Pfrommer, B. G., Cote, M., Louie, S. G. & Cohen, M. L. Relaxation of crystals with the quasi-Newton method. *J. Comput. Phys.* **131**, 233-240 (1997).

16 Rappe, A. M., Rabe, K. M., Kaxiras, E. & Joannopoulos, J. D. Optimized pseudopotentials. *Phys. Rev. B* **41**, 1227-1230 (1990).

17 Monkhorst, H. J. & Pack, J. D. Special points for Brillouin-zone integrations. *Phys. Rev. B* **13**, 5188-5192 (1976).

18 Frisch, M. J. *et al.* Gaussian 09, R. B. Gaussian, Inc., Wallingford CT (2009).

19 Lu, T. & Chen, F. Multiwfn: A multifunctional wavefunction analyzer. *J. Comput. Chem.* **33**, 580-592 (2012).